Appl Phys B (2011) 103:847–852
DOI 10.1007/s00340-010-4300-7

Applied Physics B
Lasers and Optics

Optically stimulated heating using Nd^{3+} doped $NaYF_4$ colloidal near infrared nanophosphors

A. Bednarkiewicz · D. Wawrzynczyk · M. Nyk · W. Strek

Received: 13 August 2010 / Revised version: 21 October 2010 / Published online: 17 December 2010

Abstract Although efficient in heat generation, gold nanoparticles dedicated for photostimulated localized hyperthermia treatment (LHT) lack luminescent properties suitable for detection in heterogeneous and autofluorescent tissue. Here, we study and report the use of bifunctional luminescent neodymium (Nd^{3+}) ions doped α-$NaYF_4$ colloidal nanoparticles as potential nanoheaters suitable for LHT. Up to 35°C (0.8°C/mW@514.5 nm) temperature rise in ∼0.5 ml colloidal 25%Nd^{3+}:$NaYF_4$ solution was achieved in comparison to around a 4°C rise for the undoped colloidal $NaYF_4$. The maximum temperature (T_{max}) was linearly proportional to the concentration of Nd^{3+} dopant. The time required to elevate temperature to $1/e \times T_{max}$ varied from 100 to 135 seconds. The proposed approach gives premises to the construction of multi-functional therapeutic agents detectable by means of fluorescence molecular imaging.

A. Bednarkiewicz (✉) · W. Strek
Institute of Low Temperature and Structure Research, PAN, ul. Okolna 2, 50-422 Wroclaw, Poland
e-mail: a.bednarkiewicz@int.pan.wroc.pl
Fax: +48-71-3441029

W. Strek
e-mail: w.strek@int.pan.wroc.pl

D. Wawrzynczyk · M. Nyk
Institute of Physical and Theoretical Chemistry, Department of Chemistry, Wrocław University of Technology, ul. Wybrzeże Wyspiańskiego 27, 50-370 Wroclaw, Poland

D. Wawrzynczyk
e-mail: dominika.wawrzynczyk@pwr.wroc.pl

M. Nyk
e-mail: marcin.nyk@pwr.wroc.pl

1 Introduction

Back in 1868, live *Streptococcus pyogenes* bacteria were purposely administrated by Professor Busch to a *sarcoma* cancer patient. The bacterial infection initiated a few days lasting 40°C fever leading to a spectacular tumor regression [1, 2]. Since then, many studies have been conducted in order to understand the role of heat treatment (contemporary Hyperthermia (HT) therapy) in tumor regression. The HT treatment has proven to destroy tumor tissues (through stimulation of T cells, activation of NF-κB transcription factors, release of heat shock proteins, increased immunogenic HSP90 peptide displaying on cancer cells, activation of natural killer cells [3]) or enhance the other tumor treatment methods (like radiotherapy or chemotherapy) [4, 5]. Despite advantages, the whole body fever is highly exhausting for humans and not easy to manage. Focusing light energy or radio-frequency energy on specific organs may provide better treatment control but in general spatial localization of the thermoablation is not sufficient, making it difficult to avoid medically/cosmetically unacceptable destruction of healthy surrounding tissues.

A significant improvement in the management of HT treatment has been achieved with a LHT treatment [6–8]. The LHT relays on the introduction of small, nanometer-size particles that are responsible for converting the delivered energy (i.e., photons, magnetic field) into heat, which is further transferred to the surrounding cells/tissue. The spatial localization is usually achieved by biofunctionalization of the nanoparticles (NPs) surface with antigens [7, 9, 10]. Biofunctionalized gold nanostructures (nanorods [11], nanocubes [12], nanocages [13, 14], nanoshells [15] as well as hybrid Au-Fe3O4 [16]) or graphene [17] have been successfully applied as nanoheaters in many in-vitro studies and allowed to diminish most of the drawbacks of the

original method. However, cetyltrimethylammonium bromide (CTAB) used as gold nanostructures surfactant and stabilizer, demonstrated inherent toxicity. Moreover, while being able to produce heat upon illumination with NIR (∼800 nm) optical radiation, the gold nanostructures exhibit broad (FWHM ∼150 nm) emission only under UV-green excitation and very weak emission under two photon excitation [14]. Thus, for any kind of the treatment monitoring by optical methods, additional fluorophores need to be covalently attached to the gold NPs. For that purpose, ∼156 nm large multifunctional hyperthermal nanoparticles (HTNP) have been synthesized [4]. Poly(styrenesulfonate)-coated Au nanorods photothermal NPs have been combined with Taxol loaded PLGA NPs, Fe_3O_4 magnetic resonance contrast NPs (6 nm), and luminescent quantum dots (12 nm). The HTNP could be excited either with optical or radio frequency radiation which penetrates deeper through the tissue. The treatment monitoring could be performed with MRI imaging, which apart from inconvenience for the patient, is a very expensive imaging technique.

In the present paper, we propose a new idea and demonstrate for the first time the application of a colloidal solution of bifunctional Nd^{3+} doped $NaYF_4$ nanoparticles to heat large volumes of sample. Although rare earth Er^{3+}/Yb^{3+} codoped up-converting GaN [18], $NaYF_4$ [19] or Gd_2O_3 [20] nanoparticles (UCNs) powders have already indicated increased heating of their surrounding in air or in bulk samples, we demonstrate the use of NIR excitation—Stokes NIR luminescent colloidal phosphors to heat substantially large volumes, which give premises to use them for localized photothermotherapy and bioimaging in parallel.

2 Experimental methods

All chemicals necessary for hydrothermal synthesis were used without further purification. Acetone (CH_3COCH_3), Hexane (C_6H_{14}), Ethanol (C_2H_5OH), and Chloroform ($CHCl_3$) were purchased from POCH S.A. Oleic acid ($C_{18}H_{34}O_2$), Octadecen ($C_{18}H_{36}$), and Trifluoroacetic acid ($C_2HF_3O_2$) from ALDRICH Chemistry. However, Sodium trifluoroacetate ($C_2F_3NaO_2$) was purchased from Fluka Analytical. Yttrium (III) oxide (Y_2O_3) and Neodymium (III) oxide (Nd_2O_3) were purchased from Alfa Aesar.

NPs were synthesized via a thermal decomposition reaction of trifluoroacetate precursor in mixture of technical grade chemicals, octadecene, and the coordinating ligand oleic acid. The procedure is well established in the literature [13, 21]. In a typical synthesis, fixed amounts of Nd_2O_3 and Y_2O_3 were mixed with 50% aqueous trifluoroacetic acid and heated to 90°C to obtain lanthanide trifluoroacetate precursors. The residual solvents were evaporated using a rotary evaporator. Next, the obtained trifluoroacetate precursor salt was added to three-necked flask with octadecene, oleic acid, and sodium trifluoroacetate. The solution was then heated to 110°C under vacuum with stirring for 20 minutes to remove water and oxygen, during which the flask was purged with dry argon every 5 min. The resulting yellow solution was then heated to 300°C under argon and kept under vigorous stirring for at least 1 h. After synthesis, the mixture was cooled to room temperature, precipitated by acetone, collected by centfiguration at 5,000 rpm for 10 min, and washed several times with ethanol. Finally, the entire quantity of NPs was directly dispersed in chloroform (5 ml).

XRD measurements were performed to identify the crystal structure. Patterns were recorded on a STOE diffractometer with Ge-filtered CuKα radiation. The morphology of the samples were examined by transmission electron microscopy (TEM), using a JEOL JEM-100cx microscope at an accelerating voltage of 80 kV. The UV–VIS absorption spectra were measured using spectrophotometer (Varian CARY 5E UV–Vis–NIR) with a wavelength ranging from 400 to 950 nm and resolution of 0.1 nm. The emission spectra were obtained under 514.5 nm excitation of Ar–Xe ILM 120 laser, and the signals were detected by a CCD camera (Synapse HORIBA JOBIN YVONE). Fluorescence decays curves of $^4F_{3/2}$ level were recorded with photomultiplier (HAMMAMATSU R928) under 532 nm excitation of YAG:Nd LOTIS TII laser. Curves were observed and recorded on Le Croy Wave Surfer 425 oscilloscope. The temperature elevation profiles were measured with type *T* thermocouple. The thermocouple was located in a glass well 2 mm below the laser excitation beam and was shielded with metal foil against direct illumination. The same experimental configuration was used for all colloidal solution. Voltage changes were registered on Metra Tronik Digital Voltometer V534. Samples were excited with 750 mW (∼2400 W/cm^2) 514.5 nm line from Ar–Xe ILM 120 laser. All the measurements were carried out at room temperature.

3 Results and discussion

The synthesized NPs were found to be α cubic phase of the $NaYF_4$ fluorides (Fig. 1a) with an average nanoparticle size equal to 30 ± 5 nm (Fig. 1b). Four intense diffraction peaks characteristic for cubic α-$NaYF_4$ can be observed and compared to a theoretical pattern for α-$NaYF_4$ (ICSD-60257). It is obvious that the obtained materials are highly crystalline in their nature, and we have received proper $NaYF_4$ materials.

Neodymium (III) ions exhibit relatively strong absorption bands (Fig. 2) both in the VIS and IR spectral region. They may be excited either by 514.5 nm of Ar^+ laser ($^4I_{9/2} \rightarrow {}^4G_{7/2}+{}^2K_{13/2}+{}^4G_{9/2}$), at 577 nm ($^4I_{9/2} \rightarrow {}^4G_{5/2}+{}^2G_{7/2}$), 733 nm ($^4I_{9/2} \rightarrow {}^4F_{7/2}+{}^4S_{3/2}$) and 796 nm

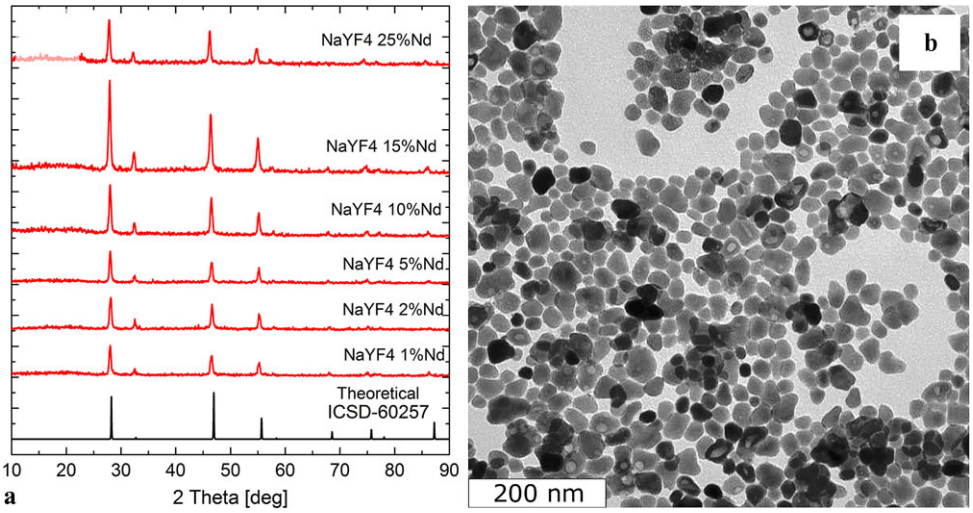

Fig. 1 Crystal structure and morphology of $NaYF_4$:Nd^{3+} NPs: (**a**) XRD patterns for $NaYF_4$ doped with different concentrations of Nd^{3+} ions, theoretical pattern is shown for reference (ICSD-60257); (**b**) Representative TEM bright image of Nd^{3+} doped $NaYF_4$

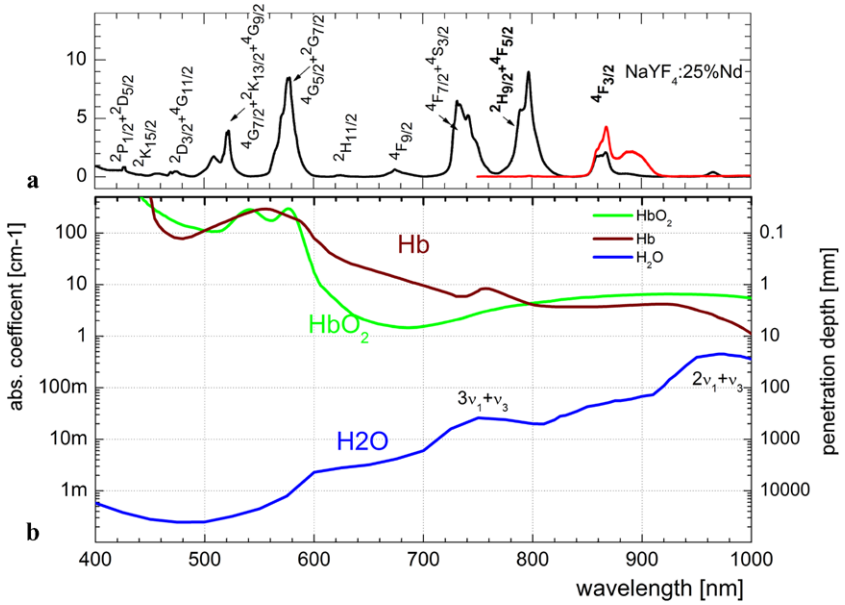

Fig. 2 Absorption coefficient of 25%Nd^{3+} doped $NaYF_4$ 2 vol.% colloidal solution (**a**) in comparison to (**b**) main human tissue absorbers (Hb, HbO_2 [22] and water [23]). Normalized $^4F_{3/2} \rightarrow {}^4I_{9/2}Nd^{3+}$ emission under 514.5 nm excitation is provided (*red curve* on **a**) for comparison

($^4I_{9/2} \rightarrow {}^4F_{7/2}+{}^4S_{3/2}$). The broadband halogen lamp is also feasible but requires higher intensities and IR filtering to avoid undesired whole body heating. Excitation with commercially available 808 nm laser diode line seems to be suitable even though the absorption coefficient is 4 times weaker than in the maximum at 796 nm. Additionally, ~808 nm line fits well with the tissue optical transmission window where low absorption coefficient of hemoglobin ($\alpha_{Hb} \sim \alpha_{HbO_2} \sim 4\ cm^{-1}$) and water ($\alpha_{H_2O} \sim 0.02\ cm^{-1}$) allows for a few centimeters deep light penetration.

The important advantage of using Nd^{3+} activated NPs for nano-thermotherapy results from the NIR excitation and NIR emission, which ensure both deep tissue excitation and deeper imaging [22, 23]. By using a high-pass ~830 nm filter, one may image the Stokes 865 nm ($^4F_{3/2} \rightarrow {}^4I_{9/2}$) luminescence of Nd^{3+} ions (Fig. 2b) to localize areas where the HTNPs accumulate. Additionally, by using NIR excitation no (or negligibly small) tissue autofluorescence is induced which guarantees a high signal-to-noise (S/N) ratio, better contrast, and higher sensitivity of bioimaging. The sensitivity and S/N may be further improved by using gated imaging/detection and exploiting the fact, the Nd^{3+} ions luminescence decays vary in the 1–300 μs range on the variation of Nd^{3+} concentration, which are a few orders of magnitude longer then the nanosecond fluorescence lifetimes typically found in organic endogenous fluorophores.

The bifunctionality, i.e. heating and luminescent properties of lanthanide doped NPs, may be further easily extended with paramagnetic gadoliniom ions (Gd^{3+}) substituting yttrium ions (Y^{3+}) for simultaneous optical and magnetic resonance imaging (MRI) [24].

The basic mechanism behind the optically induced heating in Nd^{3+} doped materials results from its energy level structure (Fig. 3a). It is well known that the increased Nd^{3+}

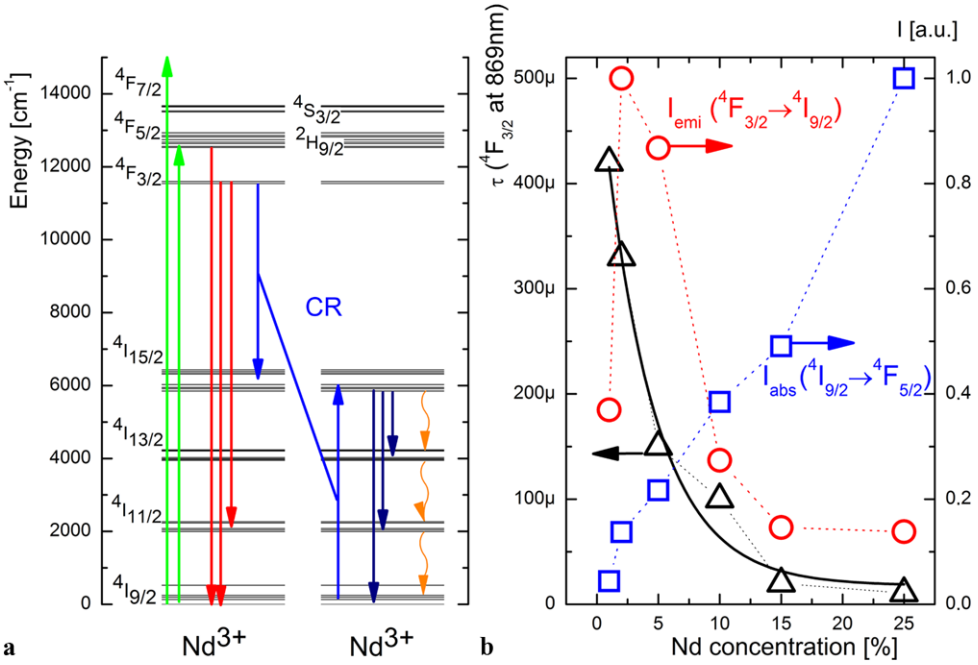

Fig. 3 (**a**) A diagram of Nd^{3+} energy levels. The arrows indicate excitation (*green*), luminescence (*red*), depopulating cross relaxation (*blue*), IR emission (*navy blue*) and nonradiative de-excitation (*orange wave arrows*). (**b**) A comparison of Nd^{3+} concentration dependent $^4F_{3/2}$ luminescence lifetimes (*black*, fitted with $y = y_0 + A\exp(-[Nd]/4.17)$ model), normalized relative $^4F_{3/2} \rightarrow {}^4I_{9/2}$ emission intensity (*red*) and integrated absorption of $^4I_{9/2} \rightarrow {}^4F_{5/2}$ (*blue*)

concentration leads to a reduced average distance between the adjacent ions which tend to nonradiatively cross-relaxate (CR). The process is described as

$$\begin{aligned}(^4F_{3/2};\ {}^4I_{9/2}) &\rightarrow (\,^4I_{15/2};\ {}^4I_{15/2}),\\ (11600;\ 0) \quad &\rightarrow (\,5851;\ \ 5851), \qquad \Delta E = +102\ \mathrm{cm}^{-1}.\end{aligned}$$

The nonradiative CR depopulates partially the excited $^4F_{3/2}$ level resulting in simultaneous luminescence intensity and lifetime decrease with the increase of Nd^{3+} concentration, while the absorption coefficient grows nearly linearly with the doping level. This behavior is observed in Fig. 3b and may help to optimize the dopant concentration for the most efficient photo stimulated temperature increase. The impact of Nd^{3+} concentration on the luminescence intensity or luminescence lifetime is of special concern, since the optical detection/localization of nanoheaters is important for diagnosis purposes.

The CR in Nd^{3+} ions has been always regarded as a parasitic process, since it prevented the achievement of population inversion to fulfill basic requirement to achieve laser action. In our case, the CR is intentionally promoted in order to efficiently populate the $^4I_{15/2}$ level of Nd^{3+} ions. Further nonradiative depopulation rates W_{JJ} between $^4I_{J=15/2-i} \rightarrow {}^4I_{J'=13/2-i}$ $(i = 0, 1, 2)$ energy levels may be calculated based on energy gap dependence [25]. For a matrix similar to ours (i.e., $LiYF_4$), one may calculate a sum of nonradiative transitions $\sum W_{JJ'} = 6.9 \times 10^5\ \mathrm{s}^{-1}$ between the intermanifold $J \rightarrow J'$ levels. The $W_{JJ'}$ describes the phonon efficiency generation in solid state material. In colloidal solutions of nanosized materials, this efficiency may be even higher due to surface effects and possibility to generate phonons both in the nanocrystallite volume and in the solvent. Another approach to increase the $W_{JJ'}$ is the change of the host matrix. The nanoheater efficiency may be easily improved by using, e.g., oxide NPs like $Y_3Al_5O_{12}$ or YVO_4, which are characterized by a higher cut-off frequency, e.g., $\sim$700 cm^{-1} for $Y_3Al_5O_{12}$ vs. $\sim$400 and 560 cm^{-1} for $LiYF_4$. This simple approach should increase the nanoradiative relaxation rate to $2.3 \times 10^{10}\ \mathrm{s}^{-1}$, which is over 3.3×10^4 times higher than that for the matrix studied here. The efficient synthesis protocols of homogenous water colloidal solution of oxide NPs have been developed [26–28] and studied for bioimaging applications.

Another interesting approach for thermotherapy may be to explore up-converting rare earth doped nanomaterials to efficiently convert near infrared light ($\sim$980 nm) to visible luminescence and simultaneously to heat. Most frequently codoping with Er^{3+}:Yb^{3+} or Tm^{3+}:Yb^{3+} is used for luminescence generation, since Yb^{3+} ions demonstrate strong NIR absorption bands and are able to up-convert the excitation photons and populate higher energy levels of Er^{3+}/Tm^{3+} ions. Meanwhile, due to a nonresonant energy transfer between the sensitizer and the active ion, excess of photon energy is converted to matrix phonons, which are responsible for the heat generation. The increase of temperature by up to 400°C in dry Er/Yb doped nanopowder and by around 90°C for bulk nanoglass-ceramics was observed under 230 mW of 976 nm NIR radiation [19]. Around a 504 K temperature increase was estimated for Er/Yb doped Gd_2O_3 nanophosphor under 290 mW excitation [20]. Simultaneously, visible anti-Stokes emission from Er^{3+} or Tm^{3+} ions may be observed and used for diagnosis

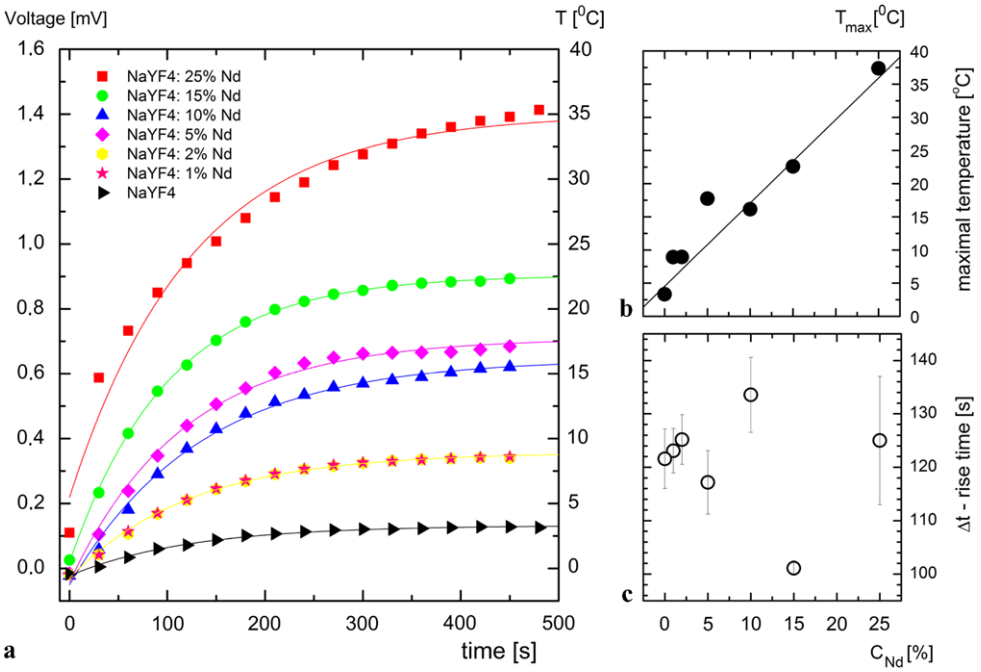

Fig. 4 (**a**) Temporal profiles of the sample's temperature vs. Nd^{3+} concentration in nano $NaYF_4$ colloidal solution, (**b**) maximum achievable temperature T_{max} [°C] and (**c**) rise times Δt [s] are presented vs. Nd^{3+} doping content

or imaging [29]. Temperature sensing has been addiotionally achieved with the Er/Yb:$NaYF_4$ system due to relative changes of the green Er^{3+} luminescence spectra shapes [30]. This feature has been rationalized by thermal Boltzman population of the well-defined energy levels. Unfortunately, the absorption coefficient of water becomes significant in the NIR/IR region around 980 nm; especially absorption bands corresponding to $2\nu_1$ (symmetrical stretching) $+\nu_3$ (asymmetrical stretching) at vibrations 980 nm reaches 0.5 cm^{-1}, whereas it is almost 21 times smaller at 808 nm [23]. Thus, the 800 nm excitation is preferred for photostimulated thermotherapy due to better spatial selectivity of the treatment. Optionally, the Yb^{3+} ions may be excited in the 920–940 nm range, but then much lower absorption coefficient reduces the quantum efficiency of the nanoheater.

Temporal profiles of temperature increase in dependence of Nd^{3+} concentration (Fig. 4a) were recorded every 30 seconds over 500 seconds to study the heat generation efficiency for a 500 µl volume of the ∼2 vol% colloidal $X\%Nd^{3+}$:$NaYF_4$ ($X = 2, 5, 10, 15, 25\%$) in $ClCH_3$ solution placed inside the cuvette. The profiles could be fitted with an exponential growth model ($y(t) = T_{max} \exp(t/\tau) + B$), to further extrapolate the maximum achievable temperature T_{max} (Fig. 4b) and assess rise time τ (Fig. 4c), i.e., time required to reach $1/e$ of T_{max}.

Over 35°C relative temperature rise of colloidal $25\%Nd^{3+}$:$NaYF_4$ solution was achieved in comparison to around 4°C for the undoped colloidal $NaYF_4$ solution. This is fairly sufficient for hyperthermia, since the rise of tissue temperature from 36.6°C up to 43°C (by ∼6°C) should already be effective. The maximum achievable temperature was linearly proportional to the concentration of Nd^{3+} dopant. The rise times did not exhibit similar correlation, and varied between 100 and 135 seconds.

The efficiency of heat generation should be addressed, since the absorption coefficient of the Nd^{3+} doped NPs and selection of the excitation line is of critical importance to achieve the best performance. The absorption coefficient varies with wavelength and is equal to $\alpha(522\text{ nm}) = 0.39\text{ cm}^{-1}$, $\alpha(578\text{ nm}) = 0.85\text{ cm}^{-1}$, $\alpha(796\text{ nm}) = 0.89\text{ cm}^{-1}$ while for the commercially available laser lines reaches $\alpha(514.5\text{ nm}) = 0.12\text{ cm}^{-1}$ and $\alpha(808\text{ nm}) = 0.22\text{ cm}^{-1}$. Since our experiment was carried with 514.5 nm laser line, only 44 mW of the 750 mW input optical power was absorbed, then converted to heat and dissipated to the surrounding volume. These values indicate the feasibility of using 4–7 times lower light intensities than in our studies, when proper excitation wavelength is selected. Further improvement by reducing the excitation light intensity may be achieved, since only 6°C temperature rise is sufficient for hyperthermia therapy. Thus, the intensities could be lower than 15–25 mW (47–80 W/cm^2), which currently is only an order of magnitude higher than for gold nanostructures [11, 14]. Yet further highly promising optimization may be carried out by application of oxide NPs instead of fluorides to significantly improve the nonradiative rates and increase heat generation efficiency. The temperature rise in HTNP treated tissues will however severely depend on the rate of accumulation of HTNP within the volumes of abnormal tissue. The selectivity and effectiveness of treatment will relay on many factors like bioconjugation of NPs, NPs drug delivery and internalization mechanism, etc. Thus, the final required light flux for Nd^{3+} doped nanoheaters is difficult to assess on the current stage of the studies.

4 Conclusions

Lanthanide (III) ions doped nanoparticles as nanoheaters have a number of advantages over traditionally used gold nanostructures. This is because a single ∼25 nm NP may provide multifunctionality. The Nd^{3+} doped $NaYF_4$ NPs may be excited in the visible (e.g., 514 nm) or near IR (∼795 nm) range exhibiting near IR emission (e.g., at ∼940 or ∼1060 nm). Thus, no severe modifications are required to traditional fluorescence detection/imaging instruments in order to study the distribution of these HTNP within the cells or tissues. Near IR excitation and emission fits the optical transmission window of the biological tissue, resulting in several-fold increased light penetration depth in comparison to UV or VIS range. Additionally, the luminescence lifetime of the $^4F_{3/2}Nd^{3+}$ level is relatively long (10–150 μs) and predictably depends on the doping concentration. The lack of spectral interference with tissue autofluorescence or the possibility to gate the observed luminescence decays make these luminophores highly attractive for bioimaging. Also, other image modalities may gain by using RE^{3+} doped NC, like OCT or MRI. And finally, due to easily controllable nonradiative transitions within lanthanides, heat loading is comparable to gold nanorods and fairly sufficient to conduct nanoparticle assisted localized hyperthermia treatments.

Acknowledgements A.B. acknowledges support from the MNiSW under Grant No. N N507 584938. M.N. and D.W. acknowledge support from the Foundation for Polish Science.

References

1. W. Busch, Berl. Klein Wochenschr. **5**, 137 (1868)
2. U. Hobohm, Cancer Immunol. Immunother. **50**, 391 (2001)
3. U. Hobohm, Br. J. Cancer **92**, 421 (2005)
4. F.Y. Cheng, C.H. Su, P.C. Wu, C.S. Yeh, Chem. Commun. (Camb.) **46**, 3167 (2010)
5. G. Baronzio, A. Gramaglia, G. Fiorentini, In Vivo **23**, 143 (2009)
6. A.H. Habib, C.L. Ondeck, P. Chaudhary, M.R. Bockstaller, M.E. McHenry, J. Appl. Phys. **103**, 07A307 (2008)
7. J.N. Shan, J.B. Chen, J. Meng, J. Collins, W. Soboyejo, J.S. Friedberg, Y.G. Ju, J. Appl. Phys. **104**, 094308 (2008)
8. A.R. Lowery, A.M. Gobin, E.S. Day, N.J. Halas, J.L. West, Int. J. Nanomed. **1**, 149 (2006)
9. M. Wang, C.C. Mi, W.X. Wang, C.H. Liu, Y.F. Wu, Z.R. Xu, C.B. Mao, S.K. Xu, ACS Nano **3**, 1580 (2009)
10. R. Abdul Jalil, Y. Zhang, Biomaterials **29**, 4122 (2008)
11. G.P. Goodrich, L. Bao, K. Gill-Sharp, K.L. Sang, J. Wang, J.D. Payne, J. Biomed. Opt. **15**, 018001 (2010)
12. X. Wu, T. Ming, X. Wang, P. Wang, J. Wang, J. Chen, ACS Nano **4**, 113 (2010)
13. J. Chen, D. Wang, J. Xi, L. Au, A. Siekkinen, A. Warsen, Z.Y. Li, H. Zhang, Y. Xia, X. Li, Nano Lett. **7**, 1318 (2007)
14. L. Au, D. Zheng, F. Zhou, Z.Y. Li, X. Li, Y. Xia, ACS Nano **2**, 1645 (2008)
15. H. Park, J. Yang, J. Lee, S. Haam, I.H. Choi, K.H. Yoo, ACS Nano **3**, 2919 (2009)
16. K. Dickson et al., Nanotechnology **21**, 105105 (2010)
17. K. Yang, S. Zhang, X. Sun, S.-T. Lee, Z. Liu, Nano Lett. Article ASAP (2010)
18. M. Nyk, A. Kuzmin, P.N. Prasad, W. Strek, C.B. de Araujo, Opt. Mater. **31**, 800 (2009)
19. V.K. Tikhomirov, K. Driesen, V.D. Rodriguez, P. Gredin, M. Mortier, V.V. Moshchalkov, Opt. Express **17**, 11794 (2009)
20. S. Singh, K. Kumar, S. Rai, Appl. Phys. B, Lasers Opt. 1 (2010)
21. M. Nyk, R. Kumar, T.Y. Ohulchanskyy, E.J. Bergey, P.N. Prasad, Nano Lett. **8**, 3834 (2008)
22. S. Prahl, http://omlc.ogi.edu/spectra/hemoglobin/
23. G.M. Hale, M.R. Querry, Appl. Opt. **12**, 555 (1973)
24. R. Kumar, M. Nyk, T.Y. Ohulchanskyy, C.A. Flask, P.N. Prasad, Adv. Funct. Mater. **19**, 853 (2009)
25. A.A. Kaminskii, *Crystalline Lasers: Physical Processes and Operating Schemes* (CRC Press, Boca Raton, 1996)
26. A. Huignard, V. Buissette, G. Laurent, T. Gacoin, J.P. Boilot, Chem. Mater. **14**, 2264 (2002)
27. V. Buissette, D. Giaume, T. Gacoin, J.P. Boilot, J. Mater. Chem. **16**, 529 (2006)
28. J.W. Stouwdam, M. Raudsepp, F.C.J.M. van Veggel, Langmuir **21**, 7003 (2005)
29. M. Wang, W. Hou, C.C. Mi, W.X. Wang, Z.R. Xu, H.H. Teng, C.B. Mao, S.K. Xu, Anal. Chem. **81**, 8783 (2009)
30. F. Vetrone, R. Naccache, A. Zamarron, A.J. de la Fuente, F. Sanz-Rodriguez, L.M. Maestro, E.M. Rodriguez, D. Jaque, J.G. Sole, J.A. Capobianco, ACS Nano **4**, 3254 (2010)